communications biology

A Nature Portfolio journal

Article

https://doi.org/10.1038/s42003-025-07955-7

G0S2 modulates normal vitreous-induced proliferation in endothelial cells

Yiwei Yin[1,2,3,10], Li Pu[1,2,4,10], Xi Yang[5,6,10], Ying Zhu[1,2], Fang Chen[7], Chenkun Wu[5,8], Hetian Lei[9] & Wenyi Wu[1,2]

Abnormal blood vessel growth in the eye is a leading cause of vision loss globally, particularly in diseases like diabetic retinopathy where the vitreous plays a crucial but poorly understood role in disease progression. While we know the vitreous can stimulate blood vessel growth, the specific molecular mechanisms remain unclear. Here we show that a protein called G0S2 (G0/G1 switch gene 2) serves as a key regulator of blood vessel growth in response to normal vitreous. Through comprehensive gene analysis, we discovered that G0S2 levels increase significantly when blood vessel cells are exposed to normal vitreous. The importance of G0S2 is highlighted by our finding that uveal melanoma patients with higher *G0S2* levels had poorer survival rates. When we removed G0S2 from blood vessel cells, they no longer responded to vitreous stimulation, confirming its critical role. Notably, we identified an existing drug that can target G0S2, potentially offering a new therapeutic approach. This discovery of G0S2's role and its potential therapeutic targeting opens new avenues for treating eye diseases characterized by abnormal blood vessel growth, while also providing a valuable biomarker for predicting disease progression in eye cancer patients.

Diabetic retinopathy, a sight-threatening complication of diabetes, is hallmarked by the proliferation of abnormal blood vessels within the retina. In parallel, ROP affects premature infants and similarly involves the aberrant growth of blood vessels in the retina. While the mechanisms underlying these neovascular processes remain incompletely understood, recent investigations have implicated the vitreous as a potential contributor. By investigating the interactions between the vitreous and endothelial cells, a better understanding of the pathogenesis of these ocular disorders can be achieved.

The vitreous, a gel-like and transparent substance occupying the posterior segment of the eye, has long been believed to lack vascularization and contain inhibitory factors against blood vessel growth[1,2]. Its primary functions include maintaining ocular shape and serving as a transparent medium for transmitting light to the retina. However, emerging research has shed light on the potential involvement of the vitreous in endothelial cell proliferation, mainly when endothelial cells breach Bruch's membrane and infiltrate the vitreous cavity—a critical process underlying abnormal blood vessel formation observed in diabetic retinopathy (DR) and retinopathy of prematurity (ROP)[3–5].

Traditionally viewed as an avascular and immunologically privileged space, the vitreous was considered inert regarding its influence on neovascularization. Nonetheless, recent studies have challenged this notion, indicating that the vitreous microenvironment may contain factors capable of stimulating endothelial cell proliferation and angiogenesis[4,5]. One such factor is hyaluronic acid, a naturally occurring glycosaminoglycan abundantly found in the vitreous. Research has demonstrated the angiogenic properties of hyaluronic acid, as it promotes endothelial cell proliferation and migration in vitro[6]. Additionally, the vitreous contains a repertoire of proteins and molecules, including fibroblast growth factors (FGFs), which further contribute to endothelial cell proliferation and facilitate the process of angiogenesis[7]. Identifying these pro-angiogenic factors within the vitreous microenvironment has significantly broadened our understanding of its role in neovascularization. It has significant implications for our ocular diseases, such as DR and ROP, characterized by pathological neovascularization.

[1]Department of Ophthalmology, Hunan Key Laboratory of Ophthalmology, Xiangya Hospital, Central South University, Changsha, China. [2]National Clinical Research Center for Geriatric Disorders, Xiangya Hospital, Changsha, China. [3]Department of Pharmacy, Shenzhen Children's Hospital, Shenzhen, China. [4]Department of Ophthalmology, Guiyang Aier Eye Hospital, Guiyang, China. [5]College of Computer Science and Technology, National University of Defense Technology, Changsha, Hunan, PR China. [6]National Key Laboratory of Parallel and Distributed Computing, National University of Defense Technology, Changsha, Hunan, PR China. [7]Huan Key Laboratory of Molecular Precision Medicine, Xiangya Hospital & Hunan Key Laboratory of Medical Genetics, School of Life Sciences, Central South University, Changsha, China. [8]State Key Laboratory of High-Performance Computing, National University of Defense Technology, Changsha, Hunan, PR China. [9]Department of Ophthalmology The Third Affiliated Hospital of Xinxiang Medical University, Xinxiang, China. [10]These authors contributed equally: Yiwei Yin, Li Pu, Xi Yang. e-mail: 15200811001@163.com

Therefore, in this study, we aimed to delve into the role of the vitreous microenvironment in endothelial cell proliferation. Specifically, we sought to explore the mechanism of how the vitreous may affect the behavior of endothelial cells, leading to neovascularization in conditions such as DR and ROP. By elucidating the molecular mechanisms involved, we can gain valuable insights into the complex interplay between the vitreous and endothelial cells, potentially paving the way for novel therapeutic strategies in managing ocular neovascular diseases.

Results

Transcriptome characteristics in endothelial cells cultured under normal human vitreous conditions

To mimic the pathology microenvironment of vascular growth into vitreous in proliferative diabetic retinopathy in vitro, we first cultured human umbilical vein endothelial cells (HUVECs) in normal human vitreous (HV) treatment, with phosphate-buffered saline (PBS) serving as the control. The growth curves of HUVECs were monitored at each passage to assess their proliferative capacity. Previously, we observed that HUVECs cultured in normal rabbit vitreous exhibited robust proliferation[4,5]. However, the underlying molecular mechanisms driving this effect remained unclear. Therefore, we performed RNA sequencing (RNAseq) to identify potential pathways involved in cell proliferation.

As expected, we identified a total of 686 differentially expressed genes (DEGs) (318 upregulated and 368 downregulated) in the vitreous treatment group compared to the PBS control (Fig. 1a). Subsequently, we conducted enrichment and pathway analyses using Gene Ontology (GO), Kyoto Encyclopedia of Genes and Genomes (KEGG), and Reactome databases. The GO analysis revealed the enrichment of differentially expressed genes involved in inflammatory responses (Fig. 1b), and additional details regarding the 52 most significant terms in biological processes (BP), molecular functions (MF), and cellular components (CC) could be found in Fig. 1b. KEGG and Reactome pathway enrichment analyses explored the signaling pathways associated with the differentially expressed genes. The results demonstrated that the most significantly enriched pathways were related to cytokine-cytokine receptor interaction (Fig. 1c) and Signaling by Interleukins (Fig. 1d). Furthermore, we investigated the disease associated with HV-stimulated gene expression by using the disease ontology (DO)[8] and disease gene network (DisGeNET)[9], and we found hypertension (Fig. 1e), inflammation, and vascular disease (Fig. 1f) were more related.

These findings provide insights into the transcriptome characteristics of endothelial cells (ECs) cultured in the presence of normal human vitreous, highlighting the involvement of various signaling pathways and potentially associated disease in the gene expression profile.

G0S2 is significantly upregulated in retina endothelial cells with vitreous

Next, we explored the specific modulatory effect of HV-induced proliferation on human retina endothelial cells (HRECs). We treated HRECs with normal HV and applied RNA-seq, then we took the intersection of DEGs and got 19 genes in both DEGs (Fig. 2a). Next, we focused on the role of these DEGs and explored their efficacy as a prognostic biomarker in different cancers from the TCGA database. Pathological angiogenesis is central to both proliferative retinal diseases and cancer progression. Given these parallels in vascular pathology, cancer databases provide valuable insight into genes regulating blood vessel growth, making them a useful resource for studying retinal neovascularization.We first look at the TCGA-UVM cohort; patients in the high expression of *G0S2* (G0/G1 switch gene 2) group (above the median value of gene expression) had significantly shorter overall survival (OS) than those in the low expression group (HR = 3.9, $p = 0.0042$) (Fig. 2b) and the other DEGs show in Supplement table 1.

Then, we examined *G0S2* expression in other cancer patients' survival, and the results showed that four cancers had significant differences (Supplement Fig. 1). We wonder if the difference expression of *G0S2* be verified in the ocular clinical sample. Thus, we select retina endothelial cells and fibrovascular membranes of proliferative diabetic retinopathy patients. We downloaded the GSE60436 and GSE102485 datasets and examined the *G0S2* mRNA[10,11]. As shown in Supplement Fig. 2, *G0S2* was expressed and showed no difference compared with retina endothelial cells. However, we notice that the upregulation of *G0S2* was much more significant in HREC with normal vitreous treatment (Fig. 2c), and angiogenesis (*PTPRB, SH2D2A, ANGPT1, RAMP2*) enrichment suggests their potential contribution to ECs proliferation under normal vitreous conditions (Fig. 2e).

We did a protein-protein network using the STRING website, which supports the functional discovery of *G0S2* in transcriptional regulation (Fig. 2d). TBL1XR1 (Transducin Beta Like 1 X-Linked Receptor 1) functions as a transcriptional coregulator, and NCOR2 (Nuclear Receptor Corepressor 2) acts as a transcriptional corepressor[12]. This interaction suggests G0S2 may participate in transcriptional repression pathways. PPARA is a nuclear receptor that regulates lipid metabolism and energy homeostasis and participate in angiogenesis related disease[13]. Understanding the G0S2-PPARA axis could provide additional therapeutic targets. We believe this analysis strengthens our understanding of how G0S2 promotes endothelial cell proliferation through its interaction.

G0S2 mediates endothelial cell proliferation and vitreous response

To validate these RNA-seq results, we performed quantitative real-time PCR (QRT-PCR) analysis of *G0S2* expression. The data showed an agreement in the expression levels of these genes between the RNA-seq and Q-PCR analyses (Fig.3a). We further confirmed that protein expression of G0S2 was higher in normal human vitreous treat cells (Fig. 3b, c). This result suggests that G0S2 could regulate vitreous-induced proliferation in HREC.

Since G0S2 is upregulated in vitreous-stimulated HRECs, we investigated whether G0S2 is involved in normal human vitreous-stimulated proliferation. We used lentivirus-mediated CRISPR for G0S2 depletion in HRECs (Fig. 3d). We treated cells with vitreous for 24 hours. As shown in Fig. 3e, the knockdown of G0S2 markedly decreased the proliferation of HRECs to vitreous treatments as determined using cell number counting.

Notably, the depletion of G0S2 decreased HV-induced migration (Fig. 3f, g) and tube formation (Fig. 3h, i). These results demonstrate that G0S2 is critical in HV-stimulated cellular responses in vascular ECs.

High-performance computing-empowered discovery of potential G0S2 inhibitor

As we identify an elevated G0S2 expression level within HV treatment. We wonder whether G0S2 can be a therapeutic target in preventing HV-induced endothelial proliferation. However, there was no proper inhibitor target G0S2.

To find a latent drug that prevents G0S2 from increasing, we apply BioNet[14] to predict the potential chemical-gene interactions that affect G0S2 function. Figure 4a shows a partial schematic. C and G are primary nodes, while P and D are secondary. Edges involving secondary nodes and same-type nodes (C-C, G-G) provide auxiliary info. Core edges (C-G) is multi-relation and crucial for prediction. We classified edges by interaction, filtered out those with low counts, and retained 65 C-G interaction types (Fig. 4d).

Among the large-scale heterogeneous biological interaction network constructed with chemical, gene, biological pathway, and disease datasets, we obtained 49 FDA-approved chemicals that may affect G0S2 function (Prediction score (PSc) > 0.7), with dexamethasone predicted in our top list (PSc = 0.713) (Fig. 4b). All potential drugs are shown in Fig. 4e and Supplementary Data 1. In addition, data from the original database also indicate that dexamethasone affects the expression of G0S2. In conclusion, we next test the predicted drug to decrease G0S2 and prevent HV-induced proliferation. Alternatively, the decreasing ability suggests that dexamethasone might be a novel candidate that prevents vitreous-induced proliferation through G0S2 expression, thereby providing a possible cure therapeutic option for diabetic retinopathy.

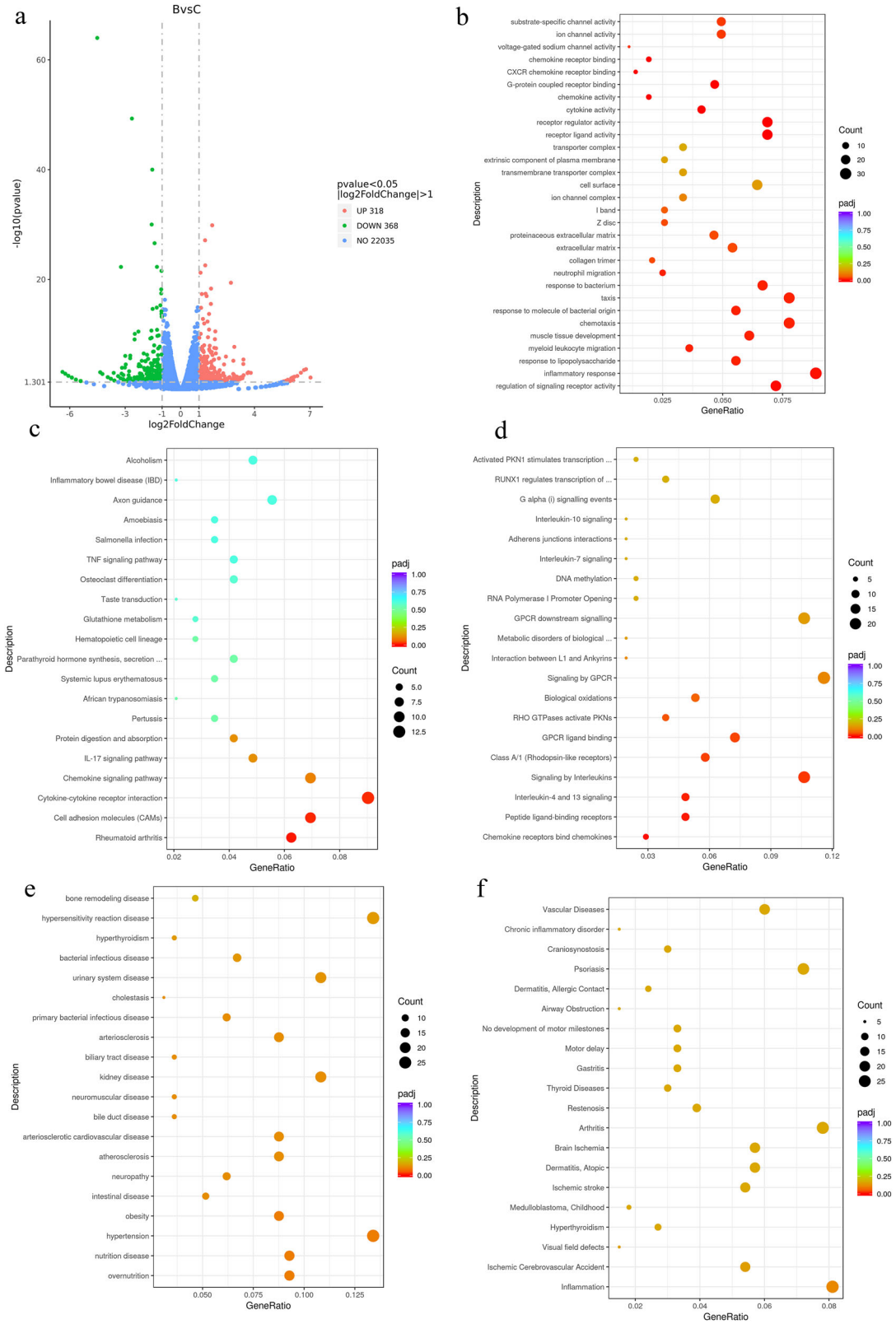

Fig. 1 | RNA sequence of the normal vitreous stimulate HUVECs. a The volcano plots showed 686 differential expressions gene (DEGs) between them and the control group (pajd<0.05, log2 (fold change) | >1), 318 genes upregulate in red dots, and 368 genes down-regulate in green dots. **b** Enrichment of DRGs in GO database ($p < 0.05, q < 0.05$). **c** Enrichment of DRGs in the KEGG database ($p < 0.05, q < 0.05$). **d** Enrichment of DRGs in Reactome database ($p < 0.05, q < 0.05$). **e** Enrichment of DRGs in the DO database ($p < 0.05, q < 0.05$). **f** Enrichment of DRGs in the DisGeNET database ($p < 0.05, q < 0.05$).

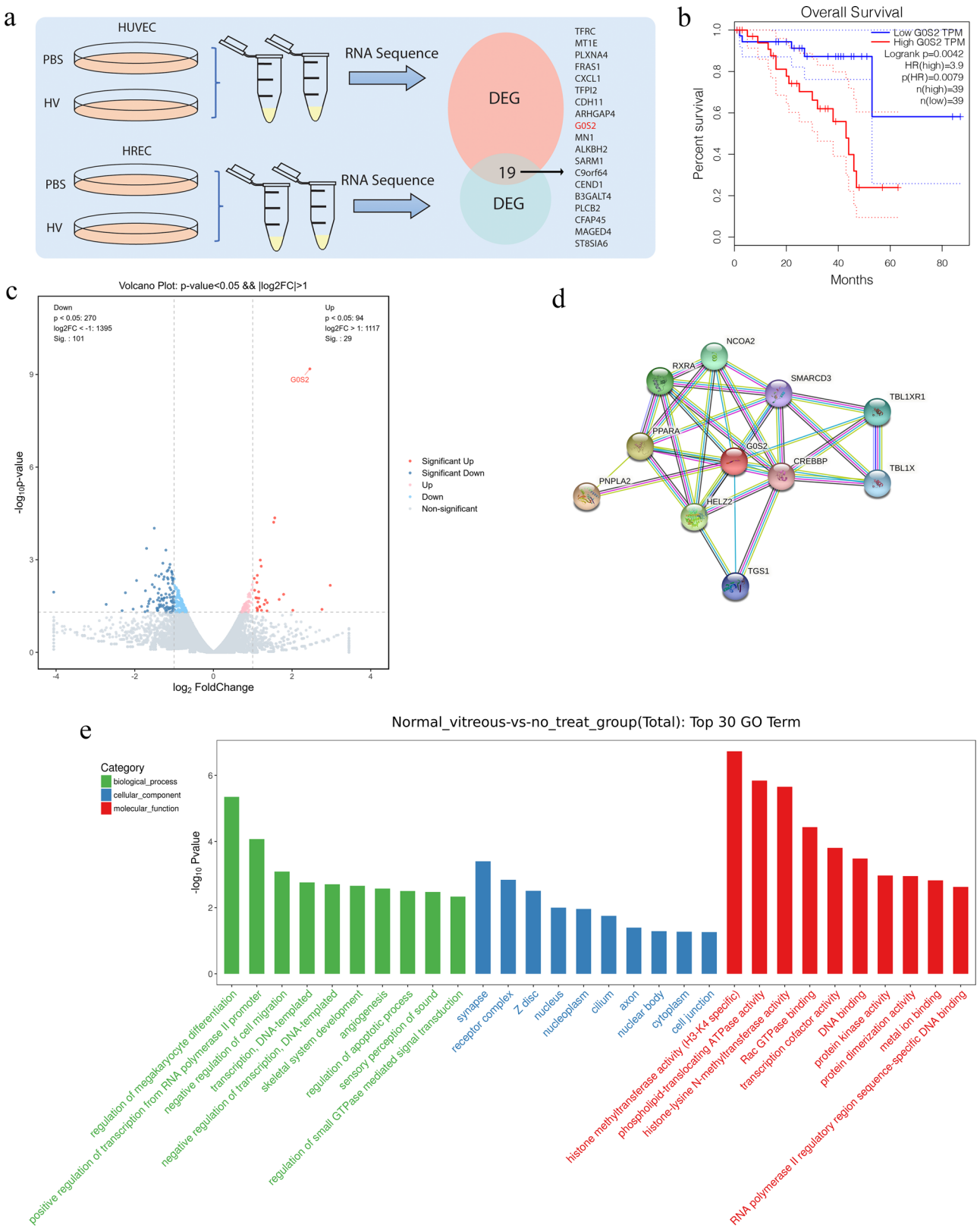

Fig. 2 | Experiment design and bioinformatic analyses indicate angiogenesis related to vitreous stimulation. a In our experiment design schematic diagram, we found 19 genes in the intersection of normal vitreous treatment in HUVECs and HRECs. **b** Kaplan–Meier survival curve of patients with high and low expression of G0S2, patients with low G0S2 expression (blue line) had significantly higher OS than those with high expression (red line) in the Uveal melanin patient TCGA database. **c** The volcano plots showed that G0S2 was upregulated in normal vitreous treatment in HREC (pajd<0.05, log2 (fold change) | >1). **d** The protein-protein interaction (PPI) network of G0S2 using the STRING website. **e** Enrichment of DRGs in HRECs with GO database ($p < 0.05$, $q < 0.05$).

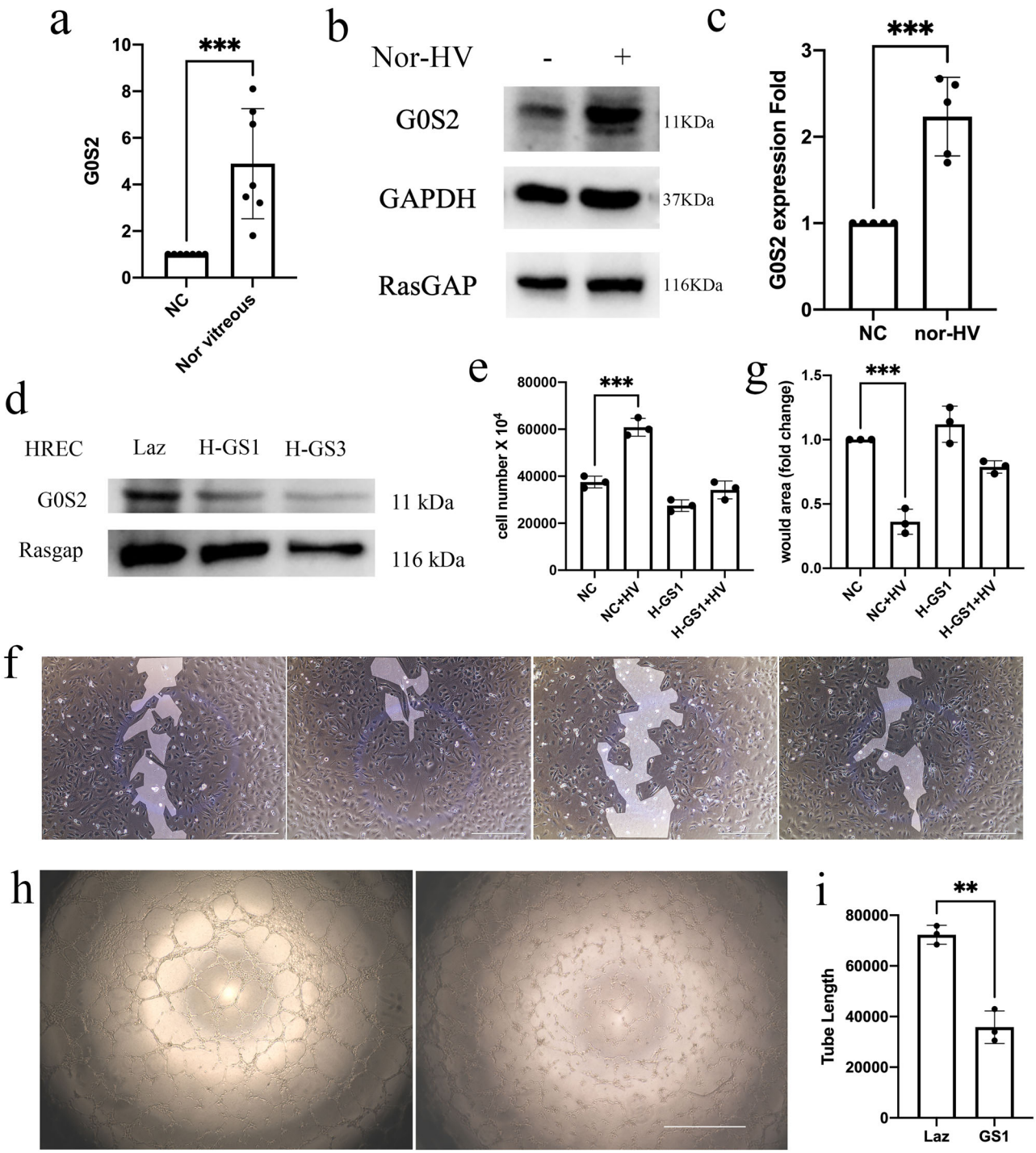

Fig. 3 | Knockdown of G0S2 prevent HV-induced angiogenesis in-vitro. a RNA expression of HV treatment in HREC. The cells were treated with normal HV for 24 hours, then lysis in triazole, following the protocol of RNA isolation and reverse transcription to cDNA. Expression of G0s2 shows a significant difference $n = 7$, $p = 0.0009$. **b** protein expression of normal HV treat with HREC for 24 hours. **c** WB quantification of HV treatment of HREC, representative of three independent experiments, $n = 5$, $p = 0.003$. **d** Depletion of G0S2 using CRISPR and G0S2 expressing of HRECs transfected with lentivirus expression SgRNA targeting lacZ or G0S2. **e** proliferation tests by cell number counting, the cells were trypsin detached and then counted in a hemocytometer under a light microscope $n = 3$. **f** A wound was created by scraping the cell monolayer with a sterile pipette tip. At 24 h post-wounding, the wound was photographed under a microscope. Scale bar 5 400 mm. **g** Quantification of migration assay, representative of three independent experiments. h. Matrigel assay to assess the tube formation of HRECs induced by vitreous with G0S2 knock-down. **h** Representative photos of three independent experiments for tube formation, Scale bar: 1000μm; **i** Bar graphs of tube lengths of three independent experiments. **means the difference was significant and $p = 0.001$.

Blockage of G0S2 prevents vitreous-induced angiogenesis

Since HV stimulates endothelial cell proliferation and participates in angiogenesis-related ocular disease, we expertly screen potential drugs that can block this signaling. Thus, we selected one potentially FDA-proven drug, dexamethasone, and tested its efficiency in cell signaling and response. To this end, we found that 1 μM dexamethasone, a potential inhibitor of G0S2, can block vitreous-induced G0S2 increasing (Fig. 5a). As expected,

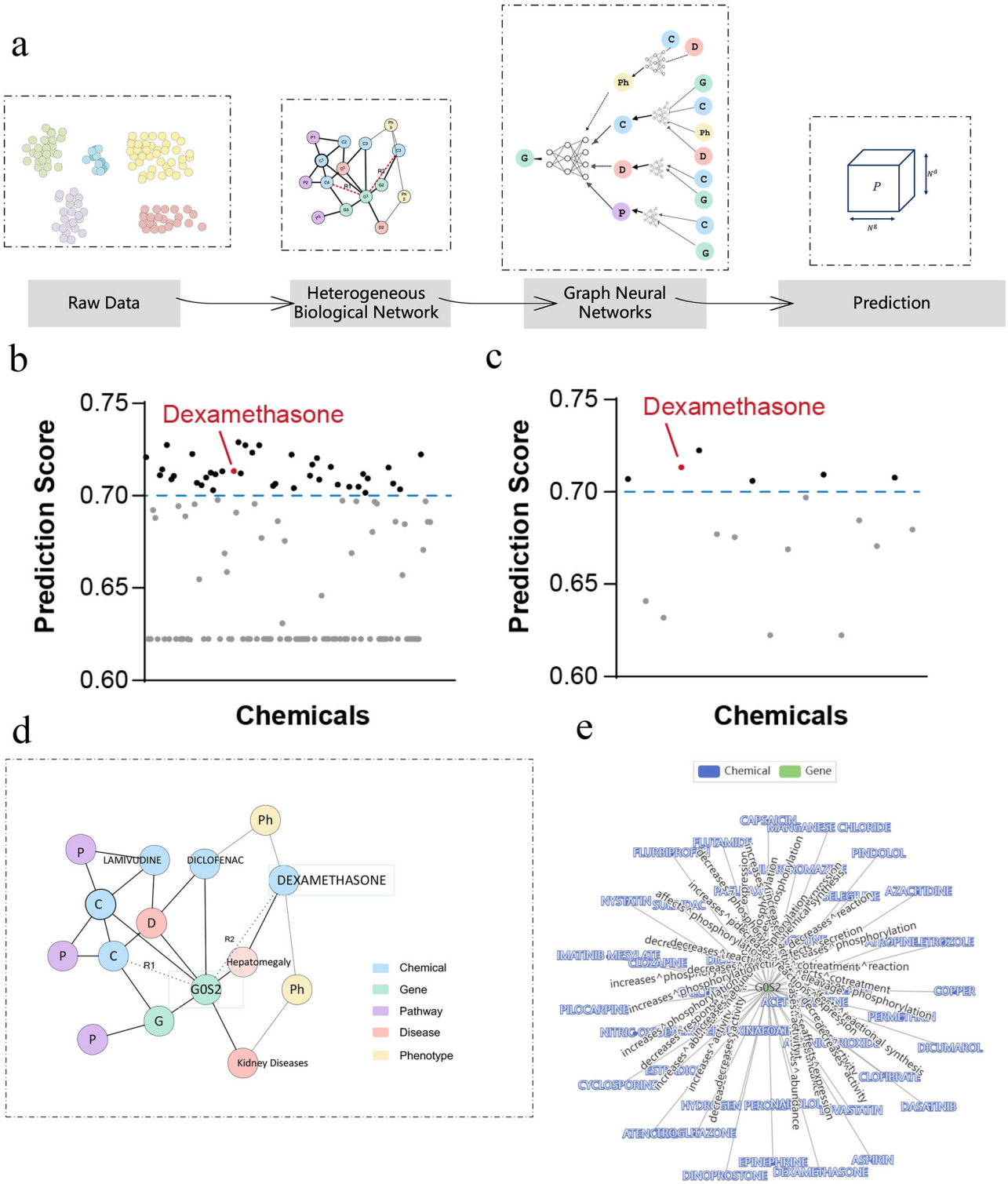

Fig. 4 | Deep learning-based discovery of potential G0S2 inhibitor. a Deep learning-based discovery of chemicals with potential effects on G0S2. Schematic representation of the deep learning algorithm to discover potential relations (R1 and R2, red dashed lines) among Chemicals (green nodes) and Genes (yellow nodes) from a heterogeneous biological network integrating chemical (C), gene (G), disease (D), pathway (P)and phenotype (Ph) datasets. **b** The prediction score of the most abundant chemicals that may affect G0S2 function was discovered by BioNet. Chemicals with a Prediction score (PSc) > 0.7 were shown. **c** Prediction score of chemicals that affect G0S2 expression (Right). **d** Biological entity network correlated to G0S2 by BioNET. **e** Chemical-G0S2 interaction network predicted by BioNET.

dexamethasone inhibited vitreous-enhanced proliferation (Fig. 5b, c) and migration (Fig. 5d, e), suggesting that targeting G0S2 by dexamethasone is a potential therapy to decrease abnormal retinal angiogenesis.

G0S2 might be the downstream of Gas6/Axl pathway

We investigate the upstream of HV, which induces G0S2 activation, so we apply bioanalysis with DEG using regression on expression levels and notice that Gas6 was related to G0S2, which might be upstream (Supplement

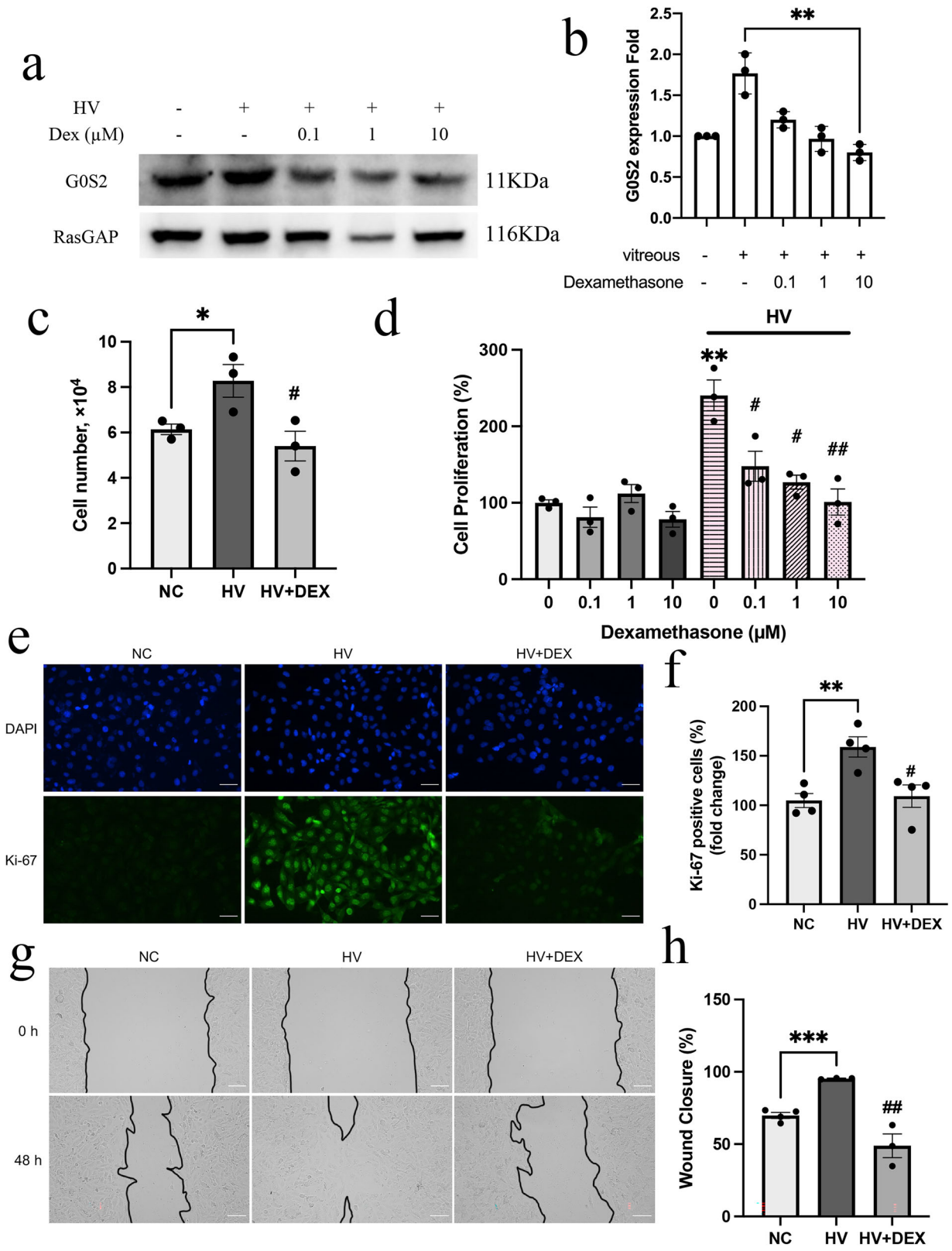

Fig. 3). Our previous work illustrates that the proliferation of endothelial cells may be mediated by a diffusible growth factor, EGF or Gas6, through EGFR or Axl, thereby increasing the sprouting of vessels[5,15]. Here, we found that Gas6 was increased dramatically with normal vitreous treatment (Fig. 6a). Thus, we hypothesize that vitreous might activate proliferation through Gas6/Axl/ G0S2. We used Axl inhibitor R428 and found that R428 can prevent HV-induced G0S2 activation (Fig. 6b).

We further investigate whether G0S2 is downstream of PI3K/AKT in vitreous-stimulated angiogenesis, as the PI3K pathway is the most critical signaling in Axl downstream and mediate cell proliferation; we found that

Fig. 5 | Dexamethasone prevents HV-induced G0S2 expression, cell proliferation, and migration. a WB showed that dexamethasone inhibits normal human vitreous-induced G0S2 increases. HRECs were exposed to HV 24 hours after starving, and different melatonin concentrations were subjected to media and Western blot to analyze Fn1 protein expression. **b** Quantification of WB of G0S2 expression, representative of three independent experiments. **c** proliferation tests by cell number counting, the cells were trypsin detached and then counted in a hemocytometer under a light microscope, $n = 3$. **d** The inhibitory effect of Dexamethasone on the proliferation of HRECs was measured by CCK-8 assay. Cells were treated with 0, 0.1, 1, or 10 μM dexamethasone with or without vitreous for 24 h. $^{**}P < 0.01$. Data are presented as mean ± SEM, $n = 3$. **e** ki-67 staining indicates that the cell proliferation rate of dexamethasone prevents HV-induced HREC growth, Scale bar: 100 μm. **f** quantification of Ki-67 staining, representative of three independent experiments. **g** A wound was created by scraping the cell monolayer with a sterile pipette tip. The cells were treated with dexamethasone (1 mmol/L) or its vehicle. At 18 h post-wounding, the wound was photographed under a microscope. Scale bar: 50 μm. **h** Quantification of migration assay, representative of three independent experiments.

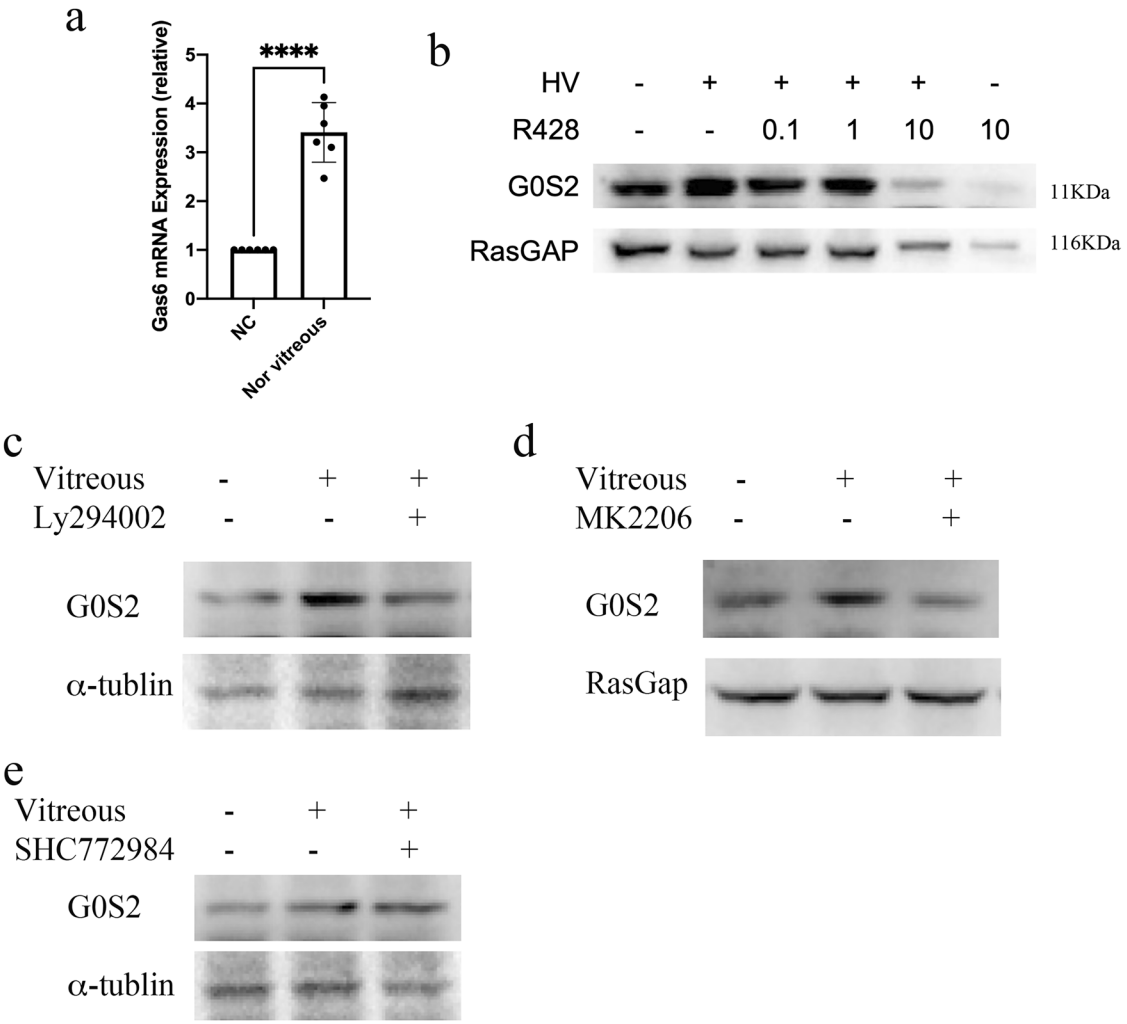

Fig. 6 | G0S2 functions as a downstream effector of Axl/PI3K/Akt pathway. a mRNA collects after normal vitreous treatment for 24 hours, and q-PCR shows the mRNA expression relative to GAPDH, $n = 6$, $p < 0.0001$. **b** WB showed that Axl inhibitor R428 prevents normal human vitreous-induced G0S2 increases. HRECs were exposed to HV 24 hours after starving, and different R428 concentrations were subjected to media and Western blot to analyze Fn1 protein expression. **c** PI3K inhibitor Ly294002 prevents vitreous-induced G0S2 activation. **d** Akt inhibitor MK2206 prevents vitreous-induced G0S2 activation. **e** Erk inhibitors cannot prevent vitreous-induced G0S2 activation.

G0S2 expression blocked by pharmacological inhibit pan-PI3K inhibitor (LY294002) and Akt inhibitor (MK-2006) at 20 nm in HV treatment (Fig. 6c, d). That means G0S2 will be downstream of the Axl/PI3K/Akt pathway. We also studied the Erk pathway inhibitor, the Axl downstream regulating cell proliferation. The data (Fig. 6e) shows that SHC772984 can't prevent the increase in vitreous-induced G0S2. Thus, we conclude that vitreous mediate endothelial cell proliferation might be through Gas6/Axl/PI3K/AKT pathway (Fig. 7).

Discussion

Vitreous factors play an important and diverse role in angiogenesis-related diseases. Prior work has shown that normal vitreous contains many growth factors, hormones, and proteins that can influence retinal and vascular physiology[16]. More importantly, the features of HV, such as spatial confinement, stiffness, stress relaxation, and fibril density, are emerging as critical signaling regulators in endothelial cells[17] when they enter the vitreous through the internal limiting membrane. However, there are conflicting reports regarding the angiogenic potential of HV phenotypes. For instance, the vitreous has been implicated in both the enhancement[5,15] and the inhibition[2] of angiogenesis. For example, pro-angiogenesis factors in vitreous have been reported to induce endothelial cell proliferation through Akt and Erk pathway in vitro assay[15]. However, the pellucid vitreous proved no vascular growth, and there might be a protein that prevents vessel growth in an in vivo study[2]. In the present study, it is widely acknowledged that

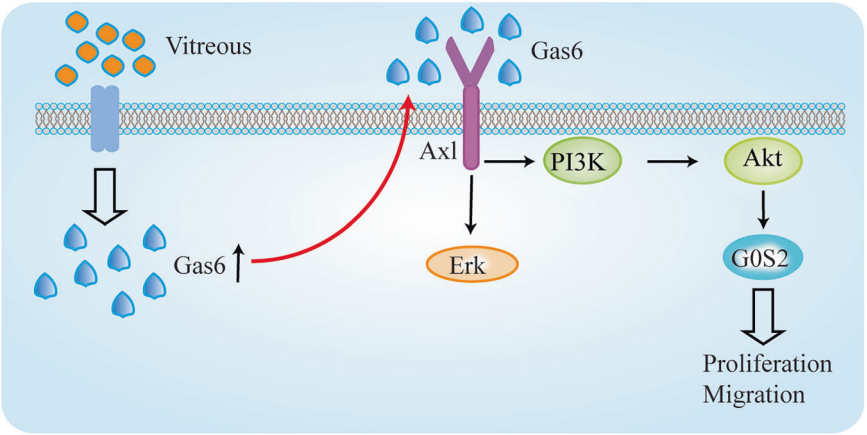

Fig. 7 | Schematic model summarizing the role of G0S2 in vitreous-induced endothelial cell proliferation. The model integrates findings from this study showing vitreous activation of G0S2 through Gas6/Axl/PI3K/AKT pathway, and the therapeutic intervention point of dexamethasone in preventing pathological angiogenesis. Known G0S2 functions from literature, G0S2 can regulate lipid metabolism by inhibits Adipose Triglyceride Lipase (ATGL) at the surface of lipid droplets and improving glucose tolerance by increased glucose uptake.

angiogenetic-related cytokines are upregulated in the vitreous of proliferative diabetic retinopathy and ischemic retinopathy. However, little literature reports the mechanism of normal vitreous stimulation of endothelial cell proliferation.

Gene expression analyses of ECs cocultured with human vitreous allowed investigation into potential pathways affected. Generally, we found that normal human vitreous promoted the expression of genes associated with the inflammatory response, cytokine-cytokine receptor interaction, and interleukin signaling, which enriches inflammation and vascular disease in the DisGeNET database. These findings are consistent with prior work demonstrating that pro-inflammatory cytokines attract immune cells, such as macrophages, to the site, induce vascular sprouting by VEGF secretion[18], and enhance tube formation of HUVECs in vitro assay[18]. Most notably, we found a gene associated with the cell cycle named *G0S2*, the most significant upregulation in normal vitreous treatment HUVECs and HRECs.

G0S2 is a crucial gene that encodes a protein that regulates cell proliferation by regulating the cell cycle, specifically in the transition from the G0 phase to the G1 phase, where cells prepare for DNA synthesis and division. Expression of G0S2 was significantly upregulated in primary human fibroblasts treated with the proapoptotic factor TNF-alpha[19]. Inhibition of NF-kappa-B abrogated G0S2 induction by TNF-alpha—moreover, G0S2 induced apoptosis by interacting with the antiapoptotic protein BCL2 in response to DNA damage. The interaction of G0S2 with BCL2 antagonized the protective effect of BCL2 by preventing the interaction of BCL2 with BAX. However, G0S2 has gained attention in cancer research due to its potential role in promoting cell proliferation in cancer cells. Elevated G0S2 expression has been observed in various cancer types, and it may contribute to uncontrolled cell growth and tumor progression[20]. A recent study shows that G0S2 can suppress breast tumors by the PI3K/mTOR pathway[21]. Our study found that G0S2 can mediate endothelial cell proliferation probably via the Gas6/Axl/PI3K/AKT pathway since we had seen that NF-kappa-B was downstream of the PI3K/Akt pathway[22].

Another role of G0S2, which focused on association with lipid droplets[23,24], raised an interesting concern that G0S2 mediating lipid droplets increased in the endothelial cell might change lipid metabolism, reminding us that lipid homeostasis is integral to endothelial cell proliferation. For this part, the upregulation of G0S2 might contribute to lipidosis in DR and AMD. G0S2 is also linked to the mitochondrial function, essential for cell energy production[25]. Since mitochondria are the cellular powerhouses responsible for energy production, we can hypothesize that vitreous-induced G0S2 activation might perturb mitochondrial function and affect cell proliferation and death in the retina cells. Thus, understanding how G0S2 influences the proliferation of endothelial cells could pave the way for novel therapeutic interventions in retina disease.

In retina angiogenesis disease, the local microenvironment had a significant effect on accelerated vascular pathology. The vitreous present-like hydrogel has the specific contribution of stress relaxation and matrix stiffness on EC functions, and the study showed that fast-relaxing coupled to low-stiffness hydrogels is positively associated with vascular sprouts[26]. This can be illustrated by the extracellular structure, which has been identified as an essential mediator in many cellular functions that support cells and regulate cell behaviors and phenotypes[27]. By targeting the factors in the vitreous that modulate endothelial cell proliferation, it may be possible to develop treatments that inhibit pathological angiogenesis while preserving the eye's normal function.

Our study has several limitations, primarily its reliance on in vitro experiments that may not fully represent the complex retinal microenvironment. The absence of animal models limits our understanding of how G0S2 functions within the blood-retinal barrier and its interactions with other cell types in vivo. Future studies should validate the Gas6/Axl/PI3K/AKT/G0S2 pathway using animal models of retinal neovascularization and explore combination approaches with existing anti-angiogenic therapies to develop more effective treatments.

Methods

Collection and preparation of normal human vitreous

Normal human vitreous was obtained from organ donors who died from accidents or trauma without any known ocular diseases during corneal donation procedures and additional informed consent were obtained from the family members of the donor. After corneal collection, the vitreous was carefully harvested, immediately snap-frozen in liquid nitrogen, and homogenized. The homogenate was centrifuged, and the supernatant was collected and stored at -80 °C until use.

Primary reagents and cell culture

Antibodies against G0S2, were purchased from Novatis (Cat:NBP1-71690) and Proteintech (cat12091-1-AP). Antibodies against Rasgap was a gift from Dr Hetian Lei's Lab, GAPDH were purchased from Santa Cruz Biotechnology (sc-47724), α-tublin from Proteintech (11224-1-AP). Secondary horseradish peroxidase (HRP) antibodies-conjugated goat anti-rabbit IgG and anti-mouse IgG were purchased from Santa Cruz Biotechnology (Santa Cruz, CA). HUVEC was a gift form cultured in Endothelial culture medium (ECM, ScienCell, cat 1001) composed of 5% Fetal Bovine Serum (FBS). HRECs were purchased from Cell System (Kirkland, WA). Cells were derived from the adult eyes of male donors. HRMECs were cultured on flasks coated with gelatin (V900863, Sigma-Aldrich) and in Endothelial Growth Medium (EGM, Lonza, Walkersville, MD) composed of 3% Fetal Bovine Serum (FBS), Endothelial Cell Growth Supplements, and penicillin/streptomycin. HRMECs were grown in average (5 mM D-glucose) and high-glucose (25 mM D-glucose) conditions. HRMECs between passage 4 (P4) and P5 were used as early passage (ep) and P11-P16 and defined as late passage (lp). The limit was reached at ≥ P20. Cells were passaged every 2–3 days and seeded at a known density (2×10^4/ml) in 24 wells. The cell counter analyzer (Cambridge Bioscience) was used for cell counts, which

stands for cell proliferation. Human embryonic kidney (HEK) 293 T cells from Xiangya Hospital were cultured in high-glucose (4.5 g/L) DMEM supplemented with 10% FBS.

Treatment conditions and RNA sequence

For RNA sequencing experiments, cells were treated with normal vitreous at a 1:3 dilution (3 mL vitreous in 6 mL serum-containing medium for a 10-cm dish) for 24 hours. Each biological replicate used vitreous from a single donor (yielding 3-4 mL per donor) to ensure consistency within experiments. Independent replicates were performed using samples from different donors.

Cell cultures in a 10 cm plate were collected with 2 ml Trizol to extract total RNA. RNA integrity was assessed using the RNA Nano 6000 Assay Kit of the Bioanalyzer 2100 system (Agilent Technologies, CA, USA). Total RNA was used as input material for the RNA sample preparations. The clustering of the index-coded samples was performed on a cBot Cluster Generation System using TruSeq PE Cluster Kit v3-cBot-HS (Illumia) according to the manufacturer's instructions. After cluster generation, the library preparations were sequenced on an Illumina Novaseq platform, and 150 bp paired-end reads were generated.

Data analysis

Raw data in fastq format were first processed through quality control. All the downstream analyses were based on clean data with high quality. Reference genome and gene model annotation files were downloaded directly from the genome website. featureCounts v1.5.0-p3 was used to count the reads numbers mapped to each gene. Then, the FPKM of each gene was calculated based on the length of the gene and read count mapped to this gene. Differential expression analysis of two conditions/groups (two biological replicates per condition) was performed using the DESeq2 R package (1.20.0). The cluster Profiler R package implemented Gene Ontology (GO) enrichment analysis of differentially expressed genes. We used the cluster profile R package to test the statistical enrichment of differential expression genes in KEGG pathways. The Reactome database brings together human model species' reactions and biological pathways. The DO (Disease Ontology) database describes the function of human genes and diseases. PPI analysis of differentially expressed genes was based on the STRING database, which known and predicted Protein-Protein Interactions.

Analysis of G0S2 in uveal melanoma

We then downloaded RNA-Seq and clinical information of 80 UM patients from The Cancer Genome Atlas data portal (TCGA) (https://portal.gdc.cancer.gov/). Kaplan Meier survival analysis was performed into two groups according to G0S2 gene expression (high and low levels, based on the median value).

Heterogeneous biological network construction

We conducted a process of selecting and integrating entity data from a diverse array of biomedical datasets, encompassing STITCH, Decagon (https://paperswithcode.com/dataset/decagon), CTD and various other reputable sources. Then built a large heterogeneous graph with five entity nodes (Chemicals, Genes, Disease, Pathway, Phenotype) and 8 relation edges (C-G, C-D, G-D, C-Ph, D-P, G-Ph, C-C, G-G).

Graph convolutional networks encoder

The graph encoder iteratively aggregates and transforms network information. We divided the graph into 7 binary-relation and 1 multi-relation subgraphs based on edge types. Nodes of each entity class are represented in an entity matrix, queryable by one-hot vectors. Binary-relation subgraphs use adjacency matrices; multi-relation subgraphs use multiple due to diverse interactions.

Prediction

Utilizing the bilinear model of BioNet, potential semantics are captured by assigning each entity a vector. This approach is well-suited for analyzing inherent asymmetric relationships, particularly those between chemicals and genes. Relations are represented as matrices that simulate interactions between potential factors. The decoder then encodes the entire knowledge graph into a 3D tensor, which can be decomposed into a core tensor and a factor matrix. In this decomposition, each 2D matrix slice within the core tensor signifies a specific relationship, while each row in the factor matrix corresponds to an entity. Given the chemical substance $v_i \in \{Vc\}$ and the gene $v_j \in \{Vg\}$, the decoder will generate the probability p_r^{ij} of the edge $e_{ij} = (v_i, r, v_j)$, which is used to calculate the likelihood of the chemical substance vi causing the type r of gene v_j interaction.

Based on the node embeddings z_i and z_j acquired by the encoder, the decoder calculates a score $G(z_i, r, z_j)$ for the edge e_{ij} and subsequently applies a sigmoid function σ to this score, as outlined below:

$$G(z_i, r, z_j) = z_i^T \quad Rz_j$$

$$p_r^{ij} = \sigma(G(z_i, r, z_j)),$$

R is a comprehensive global parameter matrix encompassing all interaction types, facilitating the sharing of information among diverse interaction categories within the mode.

Finally, we employ a straightforward result conversion code to transform matrix numerical outcomes into chemical-gene relationship pairs, subsequently ranking these results according to the PSc.

We implement BioNet by the pytorch deep learning framework (The code and data of BioNet are available at: https://github.com/yangxi1016/BioNet/), the /prediction/ folder contains code and methods for predicting the relevant entities of genes and chemicals in the database.

DNA constructs

The three 20nt target DNA sequences preceding a 5′-NGG PAM sequence in the genomic G0S2 locus were selected for generating single-guide RNA (sgRNA) for SpCas9 targets using the CRISPR design website (https://chopchop.cbu.uib.no). SgRNA for GS1: CTAGGAGGCGTGCTGCCGGT, GS3: ATGGTGAAGCTGTACGTGCT. We selected three target sequences, and the control sgRNA sequence was designed to target the lacZ gene from Escherichia coli. The lentiCRISPR v2 vector was purchased from Addgene (Cat. 52961) (Cambridge, MA). To express SpGuides in the targeted cells, the oligos of top oligos 5' -CACCG-20nt (target G0S2 DNA sequences A1, 2 3, or the lacZ sgRNA sequence) -3' and bottom oligos: 5'-AAAC-20nt (20nt: complimentary target G0S2 DNA sequences or lacZ sgRNA sequence) -C -3' were annealed and cloned into the lentiCRISPR v2 vector by BsmB1 (New England Biolabs, Boston, MA), respectively. All clones were confirmed by DNA sequencing using a primer 5'-GGACTATCATATGCTTACCG-3' from the sequence of the U6 promoter that drives the expression of sgRNAs. Both synthesis of primers and oligos and sequencing of PCR products and clones were performed at the Shenggong (Shanghai, China).

Preparation of lentivirus

Lentiviruses were produced by triple transfection of HEK 293 T cells with pLentiCRISPRv2, psPAX2, and pVSV-G (From addgene: 52961, 12260, 8454) using Lipofectamine 3000. Incubate cells for 18 hours (37 C, 5%CO2) and change media to remove the transfection reagent and replace with 5 ml DMEM with 30%FBS for viral harvests 48 hours post-transfection. Add 50% culture medium and 8ug/ml polybrene, then 50% of the lentivirus-contained medium. The infected cells were selected in media using puromycin (Sigma) (0.5 μg/ml), and the resulting cells were examined by western blotting[28,29].

Mouse model of oxygen-induced retinopathy (OIR)

The study protocol was reviewed and approved by the Xiangya Hospital Ethics Committee. This study was conducted strictly with the principles of the Declaration of Helsinki and local legislation. C57BL/6 J litters on a postnatal day 7 (P7) were exposed to 75% oxygen for five days[30]. At postnatal

day 12 (P12), pupils were kept in room air (21% oxygen). The sex of animal we used was based on nature birth. At postnatal day 17 (P17), the mice were euthanized, and retinas were carefully removed for western blot analysis or fixed in 3.7% paraformaldehyde (PFA). Mice under 6 g of total body weight were excluded from the experiments. Each experiment was at least repeated three times in this OIR model.

Western blot analysis

HRECs at 80% confluence in a 24-well plate were deprived of serum and growth factors for continuous incubation for 6-8 hours. Then, some of these cells were pretreated with vitreous (20 μl/ml) for 24 hours with or without different inhibitors. After washing twice with ice-cold phosphate-buffered saline (PBS), cells were lysed in 1 × RIPA Lysis buffer with loading buffer and protease inhibitor. The samples were boiled for 5 minutes and then centrifuged for 1 minute at 13,000 ×g. Proteins from the centrifuged and heated samples were separated by 10% SDS-polyacrylamide gel electrophoresis (PAGE) and transferred to polyvinylidene difluoride (PVDF) membranes. Blocking for one hour in 5% non-fat dry milk in TBS with 0.1% Tween-20 (TBST), followed by incubation with primary antibodies overnight at 4 °C. Primary antibodies were made in TBST with 5% non-fat dry milk (ThermoFisher Scientific). After washing with TBST, incubated with horseradish peroxidase-conjugated (HRP) secondary antibodies for one hour at room temperature. After washing in TBST, blots were developed using a chemiluminescence HRP substrate and imaged with an instrument (SAGECREATION). Protein was extracted from separate culture plates for each replicate, experiments were repeated at least three times. Signal intensity was determined by densitometry using NIH ImageJ software[29].

Cell proliferation assay

Using a cell counter, HRECs at a density of 2×10^4 cells/well number in 24-well plates were estimated after 24 h of continuous treatment with EGM-2 with or without vitreous (1:10 dilution in EGM-2). Each experiment was performed using independent cell cultures derived from different passages. At least three independent experiments ($n = 3$) were performed as described previously.

Scratch-wound migration assay

Migration was assessed with the scratch-wound assay[31] with minor modifications. Once cells reached 90% confluence in 24-well plates, they were starved for 4–6 hours. After the cell monolayer was scraped with a sterile pipette tip (200 μl) and washed twice to remove detached cells. One scratch was generated per well and imaged on a Leica microscope every six hours for 24 hours. Images were analyzed by measuring the number of pixels in the wound area using Adobe Photoshop (Adobe Systems, San Jose, CA) and ImageJ software[32]. For each assay, results were quantitated from 3 independent experiments, and values were normalized to those obtained for control cells.

Immunofluorescence

Cells were washed in TBS three times (5 min/cycle). After washing, cells were blocked with a solution containing 2% BSA in 0.25% TBS-X for 1 hour at room temperature, followed by overnight incubation at four °C with primary ki-67 antibodies (1:500). The next day, after three washes in TBS, slides were incubated with fluorescent-labeled secondary antibodies (Thermo Scientific, 1:1000) for one hour at room temperature. Sections were washed and mounted in an antifade mounting medium (solar cat: s2100). Images were obtained by using a Zeiss Apotome microscope.

Statistical analysis

GraphPad Prism (version 9) was used for data analysis. Data are presented as mean ± standard deviation (SD) or Standard Error of Mean (SEM) from three independent experiments to show data variability. For comparisons between two groups, two-tailed Student's t-test was used. Due to small sample size ($n = 3 – 6$), individual data points are shown together with summary statistics to provide transparency in data distribution. Statistical significance was defined as $P < 0.05$, with exact P-values reported for each comparison. In figures, significance levels are indicated as follows: $^*P < 0.05$, $^{**}P < 0.01$, $^{***}P < 0.001$.

Reporting summary

Further information on research design is available in the Nature Portfolio Reporting Summary linked to this article.

Data availability

The datasets of several RNA sequences from other published papers can be obtained in GEO (GSE289204 and GSE289206)and supplement tables.

Received: 4 July 2024; Accepted: 18 March 2025;
Published online: 04 April 2025

References

1. Lutty, G. A. et al. Regulation of cell growth by vitreous humour. *J. Cell Sci.* **76**, 53–65 (1985).
2. Brem, S., Brem, H., Folkman, J., Finkelstein, D. & Patz, A. Prolonged tumor dormancy by prevention of neovascularization in the vitreous. *Cancer Res.* **36**, 2807–2812 (1976).
3. Wu, W. et al. Axl is essential for in-vitro angiogenesis induced by vitreous from patients with proliferative diabetic retinopathy. *Front. Med. (Lausanne)* **8**, 787150 (2021).
4. Wu, W. et al. Normal vitreous promotes angiogenesis via activation of Axl. *FASEB J.* https://doi.org/10.1096/fj.201903105R (2020).
5. You, M. et al. Normal vitreous promotes angiogenesi via the epidermal growth factor receptor. *FASEB J.: Off. Publ. Federation Am. Soc. Exp. Biol.* **34**, 14799–14809 (2020).
6. Pardue, E. L., Ibrahim, S. & Ramamurthi, A. Role of hyaluronan in angiogenesis and its utility to angiogenic tissue engineering. *Organogenesis* **4**, 203–214 (2008).
7. Murugeswari, P. et al. Angiogenic potential of vitreous from Proliferative Diabetic Retinopathy and Eales' Disease patients. *PloS one* **9**, e107551 (2014).
8. Schriml, L. M. et al. Disease Ontology: a backbone for disease semantic integration. *Nucleic Acids Res.* **40**, D940–D946 (2012).
9. Piñero, J. et al. DisGeNET: a discovery platform for the dynamical exploration of human diseases and their genes. *Database (Oxf.)* **2015**, bav028 (2015).
10. Ishikawa, K. et al. Microarray analysis of gene expression in fibrovascular membranes excised from patients with proliferative diabetic retinopathy. *Invest. Ophthalmol. Vis. Sci.* **56**, 932–946 (2015).
11. Li, Y. et al. Induced expression of VEGFC, ANGPT, and EFNB2 and their receptors characterizes neovascularization in proliferative diabetic retinopathy. *Invest. Ophthalmol. Vis. Sci.* **60**, 4084–4096 (2019).
12. Hu, Y. et al. The role of transducin β-like 1 X-linked receptor 1 (TBL1XR1) in thyroid hormone metabolism and action in mice. *Eur. Thyroid J.* https://doi.org/10.1530/etj-23-0077 (2023).
13. Wang, Q. et al. Cell cycle regulation by alternative polyadenylation of CCND1. *Sci. Rep.* **8**, 6824 (2018).
14. Yang, X. et al. BioNet: a large-scale and heterogeneous biological network model for interaction prediction with graph convolution. *Brief Bioinform.* https://doi.org/10.1093/bib/bbab491 (2022).
15. Wu, W. et al. Normal vitreous promotes angiogenesis via activation of Axl. *FASEB J.* **35**, e21152 (2021).
16. Skeie, J. M., Roybal, C. N. & Mahajan, V. B. Proteomic insight into the molecular function of the vitreous. *PloS one* **10**, e0127567 (2015).
17. Yi, B., Xu, Q. & Liu, W. An overview of substrate stiffness guided cellular response and its applications in tissue regeneration. *Bioact. Mater.* **15**, 82–102 (2022).
18. Sindrilaru, A. et al. An unrestrained proinflammatory M1 macrophage population induced by iron impairs wound healing in humans and mice. *J. Clin. Invest.* **121**, 985–997 (2011).

19. Welch, C. et al. Identification of a protein, G0S2, that lacks Bcl-2 homology domains and interacts with and antagonizes Bcl-2. *Cancer Res.* **69**, 6782–6789 (2009).
20. Cho, E. et al. G0/G1 Switch 2 induces cell survival and metastasis through integrin-mediated signal transduction in human invasive breast cancer cells. *Biomol. Ther. (Seoul.)* **27**, 591–602 (2019).
21. Yim, C. Y. et al. G0S2 represses PI3K/mTOR signaling and increases sensitivity to PI3K/mTOR pathway inhibitors in breast cancer. *Cell Cycle* **16**, 2146–2155 (2017).
22. Wu, W. et al. Genome editing of Pik3cd impedes abnormal retinal angiogenesis. *Hum. Gene Ther.* **34**, 30–41 (2023).
23. Lu, X., Yang, X. & Liu, J. Differential control of ATGL-mediated lipid droplet degradation by CGI-58 and G0S2. *Cell Cycle* **9**, 2719–2725 (2010).
24. Zhang, X., Heckmann, B. L., Campbell, L. E. & Liu, J. G0S2: A small giant controller of lipolysis and adipose-liver fatty acid flux. *Biochim. Biophys. Acta Mol. Cell Biol. Lipids* **1862**, 1146–1154 (2017).
25. Lee, P. H. et al. G0S2 modulates homeostatic proliferation of naïve CD8+ T cells and inhibits oxidative phosphorylation in mitochondria. *Immunol. Cell Biol.* **93**, 605–615 (2015).
26. Shayan, M. et al. Elastin-like protein hydrogels with controllable stress relaxation rate and stiffness modulate endothelial cell function. *J. Biomed. Mater. Res. A* **111**, 896–909 (2023).
27. Saraswathibhatla, A., Indana, D. & Chaudhuri, O. Cell-extracellular matrix mechanotransduction in 3D. *Nat. Rev. Mol. Cell Biol.* **24**, 495–516 (2023).
28. Lei, H. & Kazlauskas, A. Growth factors outside of the PDGF family employ ROS/SFKs to activate PDGF receptor alpha and thereby promote proliferation and survival of cells. *J. Biol. Chem.* **284**, 6329–6336 (2009).
29. Lei, H. et al. RasGAP promotes autophagy and thereby suppresses platelet-derived growth factor receptor-mediated signaling events, cellular responses, and pathology. *Mol. Cell Biol.* **35**, 1673–1685 (2015).
30. Connor, K. M. et al. Quantification of oxygen-induced retinopathy in the mouse: a model of vessel loss, vessel regrowth and pathological angiogenesis. *Nat. Protoc.* **4**, 1565–1573 (2009).
31. Liang, C. C., Park, A. Y. & Guan, J. L. In vitro scratch assay: a convenient and inexpensive method for analysis of cell migration in vitro. *Nat. Protoc.* **2**, 329–333 (2007).
32. Ruan, G. X. & Kazlauskas, A. Axl is essential for VEGF-A-dependent activation of PI3K/Akt. *EMBO J.* **31**, 1692–1703 (2012).

Acknowledgements

We thank the Biobank of Xiangya Hospital, the Department of Central Laboratory, and the Huan Key Laboratory of Molecular Precision Medicine Laboratory (Central South University) for supporting this research. This work was supported by a grant from the National Natural Science Foundation of China (82271109 to W.W; 82070989 to H.L.), Natural Science Foundation of Hunan Province (grant no. 2021JJ41030 to WW. and 2022JJ70170 to Y.Z.).

Author contributions

Yiwei Yin: Investigation, Software, Validation. Li Pu: Investigation, Software, Validation. Xi Yang: Resources, Data curation. Ying Zhu: Investigation. Fang Chen: Data curation, Visualization. Chenkun Wu: Resources, Data curation; Wenyi Wu: Project administration, Writing- Original draft preparation, Funding acquisition. Hetian Lei: revise manuscript.

Competing interests

The authors declare that they have no conflicts of interest with the contents of this article.

Ethics approval and consent to participate

The Xiangya Hospital Ethics Committee reviewed and approved the study protocol. This study was conducted strictly according to the principles of the Declaration of Helsinki and local legislation. All participants were informed about the study's purpose, procedures, potential risks, and benefits.

Consent for publication

All individual participants provided explicit consent to publish their data.

Additional information

Supplementary information The online version contains supplementary material available at https://doi.org/10.1038/s42003-025-07955-7.

Correspondence and requests for materials should be addressed to Wenyi Wu.

Peer review information *Communications Biology* thanks Ying Chen, Sukhvinder Singh and the other, anonymous, reviewer(s) for their contribution to the peer review of this work. Primary Handling Editor: Ophelia Bu. A peer review file is available.